metals

MDPI

Article

Analyzing the Sintering Kinetics of Ti12.5Ta12.5Nb Alloy Produced by Powder Metallurgy

Rogelio Macias [1], Pedro Garnica [1], Ceylin Fernandez-Salvador [1], Luis Olmos [2], Omar Jimenez [3,*], Manuel Arroyo-Albiter [2], Santiago Guevara-Martinez [3] and Jose Luis Cabezas-Villa [2]

[1] División de Estudios de Posgrado e Investigación, Tecnológico Nacional de México/I. T. Morelia, Morelia 58120, Mexico
[2] INICIT, Universidad Michoacana de San Nicolás de Hidalgo, Morelia 58060, Mexico
[3] Departamento de Ingeniería de Proyectos, Universidad de Guadalajara, Zapopan 45100, Mexico
* Correspondence: omar.aleman@academicos.udg.mx

Abstract: The focus of this work is to analyze the sintering kinetics of Ti12.5Ta12.5Nb alloy by dilatometry. The mixture of powders was achieved by mixing individual powders of Ti, Ta and Nb, which were then axially pressed. Sintering was performed at 1260 °C using different heating rates. The microstructure was determined by X-ray diffraction and scanning electron microscopy. Results show that densification is achieved by solid state diffusion and that the relative density increased as the heating rate was slow. Due to the full solubility of Ta and Nb in Ti, the relative density reached was up to 93% for all samples. Activation energy was estimated from the densification rate and it was determined that two main diffusion mechanisms were predominant: grain boundary and lattice self-diffusion. This suggests that Ta and Nb diffusion did not affect the atomic diffusion to form the necks between particles. The microstructure shows a combination of α, β and α′, and α″ martensitic phases as a result of the diffusion of Ta and Nb into the Ti unit cell. It was concluded that the heating rate plays a major role in the diffusion of Ta and Nb during sintering, which affects the resulting microstructure.

Keywords: sintering; β-Ti alloys; activation energy; martensite phases; dilatometry

check for updates

Citation: Macias, R.; Garnica, P.; Fernandez-Salvador, C.; Olmos, L.; Jimenez, O.; Arroyo-Albiter, M.; Guevara-Martinez, S.; Cabezas-Villa, J.L. Analyzing the Sintering Kinetics of Ti12.5Ta12.5Nb Alloy Produced by Powder Metallurgy. *Metals* **2023**, *13*, 1026. https://doi.org/10.3390/met13061026

Academic Editor: Mariola Saternus

Received: 31 March 2023
Revised: 14 May 2023
Accepted: 21 May 2023
Published: 27 May 2023

Copyright: © 2023 by the authors. Licensee MDPI, Basel, Switzerland. This article is an open access article distributed under the terms and conditions of the Creative Commons Attribution (CC BY) license (https://creativecommons.org/licenses/by/4.0/).

1. Introduction

Currently, advances in the field of medicine demand the constant development and improvement of materials with long-term performance when interacting directly with the human body, for example, bone implants [1]. Conventional materials fabricated from Ti and its alloys are the most widely used [2]. One of the most recommended materials for the fabrication of medical implants is Ti6Al4V alloy (Ti64), due to its excellent biomechanical characteristics [3]. Additionally, Ti64 alloy has been the subject of several studies demonstrating the reactivity of the alloying elements, such as Al and V with human body fluids, which in turn, represent a potential for damage to adjacent tissues [4,5].

To overcome the disadvantages of Ti64, Ti-based materials in combination with other alloying elements that have shown better biocompatibility than Ti, like Nb, Ta, Mo, Hf, Zr, have been proposed [6]. Besides the improvement in biocompatibility, a reduction in the mechanical strength resulted from the β-Ti phase stabilization. This is a very important issue to reduce the "stress shielding" effect generated by the difference in stiffness between bone and metallic implants. β-Ti materials with the addition of Ta, Mo and Zr have shown a reduction in the moduli to values of 55–85 GPa, almost the half of the Ti64 modulus, 110 GPa [7–10]. Nevertheless, those values remain high in comparison to the reported modulus of human bones 1–28 GPa [2]. In addition to lower mechanical strength, β-Ti alloys exhibit better corrosion resistance than α-Ti and α + β alloys [9,11], with the possibility of developing martensitic type transformations β → α′ or β → α″ [10,12]. These characteristics give the shape memory behavior and superelasticity, which will favor their

application in the biomedical field [13,14]. Due to this, research has been carried out on new β-Ti alloys whose microstructure can be adjusted by the addition of different β-stabilizing elements [12,15].

Zhou and Niinomi [3,8,16,17] demonstrated that Young's modulus can be effectively reduced by adding Ta into the Ti matrix, finding that 25% Ta is the optimum content to obtain a significant reduction to 64 GPa [8]. Additionally, Ti-Ta alloys are considered among the best for compatibility with the human body, due to their mechanical properties, physical properties, and their excellent corrosion resistance [18]. On the other hand, the development of β-Ti alloys with the addition of Ta and Nb have demonstrated that Young modulus can be reduced up to 55 GPa by controlling the processing parameters [19]. These alloys are intended to improve biocompatibility and reduce elastic modulus to promote load sharing between implant and bone [20,21].

Since Ta (16.65 g/cm^3) is almost four times denser than Ti (4.5 g/cm^3), it is necessary to find elements that can reduce the density of the final parts, without modifying the final microstructure. Thus, a third alloying element can be added into the Ti-Ta alloys with similar effect than Ta. Nb is an element that, in combination with Ti, stabilizes the β-Ti phase, and by itself, it also reduces the Young's moduli to values close to those of human bones [22]. Ti based alloys using Nb as alloying element showed low moduli by the stabilization of the β phase, and thus, the martensitic phase [23]. Likewise, the combination of Nb with the Ti-Ta system increased the possible biocompatibility of the Ti-Ta-Nb system [7,21]. Besides, as the density of Nb (8.57 g/cm^3) is lower than that of Ta, it will also reduce the weight of the final alloy. To fabricate such materials, the powder metallurgy technique is a good alternative because the final density can be controlled adjusting the sintering temperature, particle size and quantity of alloying elements [24,25].

Different studies have reported the effect of Nb as a ternary element in TiTa alloys, but they were focused on the microstructure and mechanical properties of such alloys, while this work studies the sintering kinetics of the Ti12.5Ta12.5Nb alloy. The resulting microstructure is analyzed and linked to the sintering process. Dilatometry tests were performed to determine the dominant diffusion mechanisms during solid stage sintering.

2. Materials and Methods

2.1. Sample Preparation

Ti (AP&C, Boisbriand, QC, Canada), Ta and Nb powders (CRM Jiangxi, China), with particle size distributions of lower than 20 μm for Ti and Ta and lower than 100 μm for Nb, were used to prepare the samples, see Figure 1. The shape of Ti powders is spherical, meanwhile the shape of Ta powders is irregular as is the shape of Nb powders, as can be noticed in Figure 1. A mixture of 75 wt.% Ti with 12.5 wt.% Ta and 12.5 wt.% Nb was prepared in a dry condition with the aid of a turbula mixer (WAB, Sausheim, France). The mixture was obtained after 30 min. Then, 1 wt.% of polyvinyl alcohol, PVA (Merck, St. Louis, MO, USA) was added to the powder mixture as a binder. After that, the mixture was poured into a 6 mm diameter steel die and pressed with a maximum pressure of 450 MPa with a displacement rate of 0.1 mm/min, using an Instron 1150 universal mechanical testing machine (Instron, Norwood, MA, USA). The green density of samples was estimated by measuring the volume of cylindrical samples with a digital caliper (Mitutoyo, Kanagawa, Japan) and weighting them in a balance (Ohaus, Parsippani, NJ, USA). of high accuracy (0.0001 g). The dimensions of green compacts after powder compaction were around 4 mm height and 6 mm diameter.

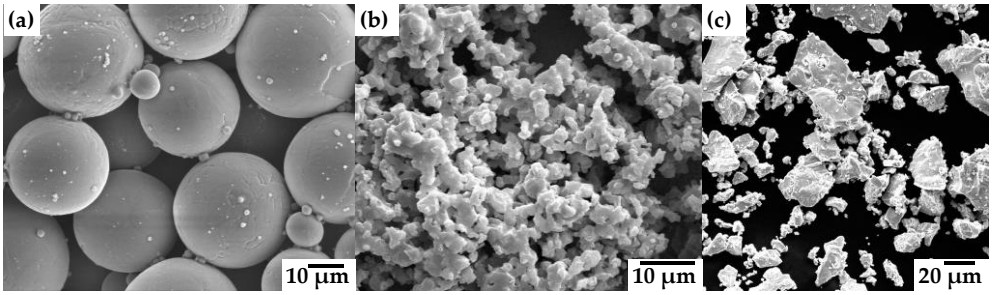

Figure 1. Initial powders (**a**) Ti, (**b**) Ta and (**c**) Nb.

Consolidation of samples was performed by sintering, but the PVA was first eliminated with a thermal cycle at 500 °C with a heating rate of 10 °C/min under high purity argon atmosphere in a L75V vertical dilatometer (Linseis, Robbinsville, NJ, USA). Then, sintering was performed using three different heating rates of 5, 15 and 25 °C/min. The sintering was achieved at 1260 °C for 1 h, with a cooling rate of 25 °C/min. The sintering temperature was set according to previous works, wherein relative densities higher than 95% were reached for Ti64, Ti and Ti64/xTa composites [10,14,22,23]. The thermal cycles were performed under inert argon atmosphere. To avoid oxidation during sintering, the dilatometer was purged beforehand for 30 min with flowing argon to start the heating of samples.

2.2. Dilatometry Data Analysis

For the analysis of sintering kinetics, the data obtained from axial displacement during the whole sintering cycle was used to estimate relative density. First, the geometrical density of any material can be obtained from:

$$\rho = \frac{m}{V} \tag{1}$$

where ρ is the density, m and V mass and volume of the compact. Assuming that m is constant, the instantaneous density can be calculated by following the volume change as follows:

$$\rho_i = \frac{m}{V_i} \tag{2}$$

In where the subscript "i" means instantaneous density and volume, respectively. The instantaneous volume depends on the densification during sintering, and it can be estimated from the dilatometry data, wherein the radial displacement is assumed to follow the same variation as the measured axial one, with a corrective factor being the final axial to radial shrinkage ratio. Thus, the instantaneous volume can be obtained from:

$$V_i = (\Delta l + l_o)(\Delta d + d_o)^2(\pi/4) \tag{3}$$

In where Δl is measured at any instant during the thermal cycle and Δd can also be obtained at any instant as was above explained. The relative density is defined as the weight density of the compact divided by the theoretical density of the fully dense alloy, which is calculated by using the rule of mixtures as follows:

$$\rho_t = f_{Ti}\rho_{Ti} + f_{Ta}\rho_{Ta} + f_{Nb}\rho_{Nb} \tag{4}$$

In where f_{Ti}, f_{Ta}, f_{Nb}, and ρ_{Ti}, ρ_{Ta}, ρ_{Nb}, are the volume fraction and theoretical density of each element. The calculated value of theoretical density for the Ti12.5Ta12.5Nb alloy was 5.24 g/cm^3, which was used for the following estimations. Therefore, the relative density (D) can be estimated during the complete sintering cycle as follows:

$$D = \frac{\rho_i}{\rho_t} \tag{5}$$

2.3. Microstructure Characterization

The sintered samples were metallographically prepared by grinding and polishing with Silicon Carbide (SiC) abrasive paper and alumina particles of 50 nm to achieve a mirror-like surface. Subsequently, the microstructure was observed under scanning electron microscopy; SEM JSM-5910LV (Jeol, Tokyo, Japan) and energy dispersive analysis; EDS (Bruker, Bremen, Germany) was performed. Likewise, XRD patterns were obtained by means of an Empyrean (Panalytical, Almelo, Netherlands) diffractometer using copper K alpha radiation with an energy of 30 kV and 30 mA, with a step of 0.2 and a time of 1 s per step in a 2θ range of 30–90°.

3. Results and Discussion

3.1. Sintering Analysis

Densification of samples heated at different rate was followed during the thermal cycle. Relative density of samples was barely the same at the beginning (77%), then, a reduction in relative density was noticed due to the thermal dilation, Figure 2a. Then, a continuous increment in relative density was observed from 686 °C, which indicates the activation of sintering. The activation temperature varied from 686 to 706 °C as the heating rate increased from 5 to 25 °C/min. This is also confirmed by a sharp increment in the densification rate in Figure 2b (point 1).

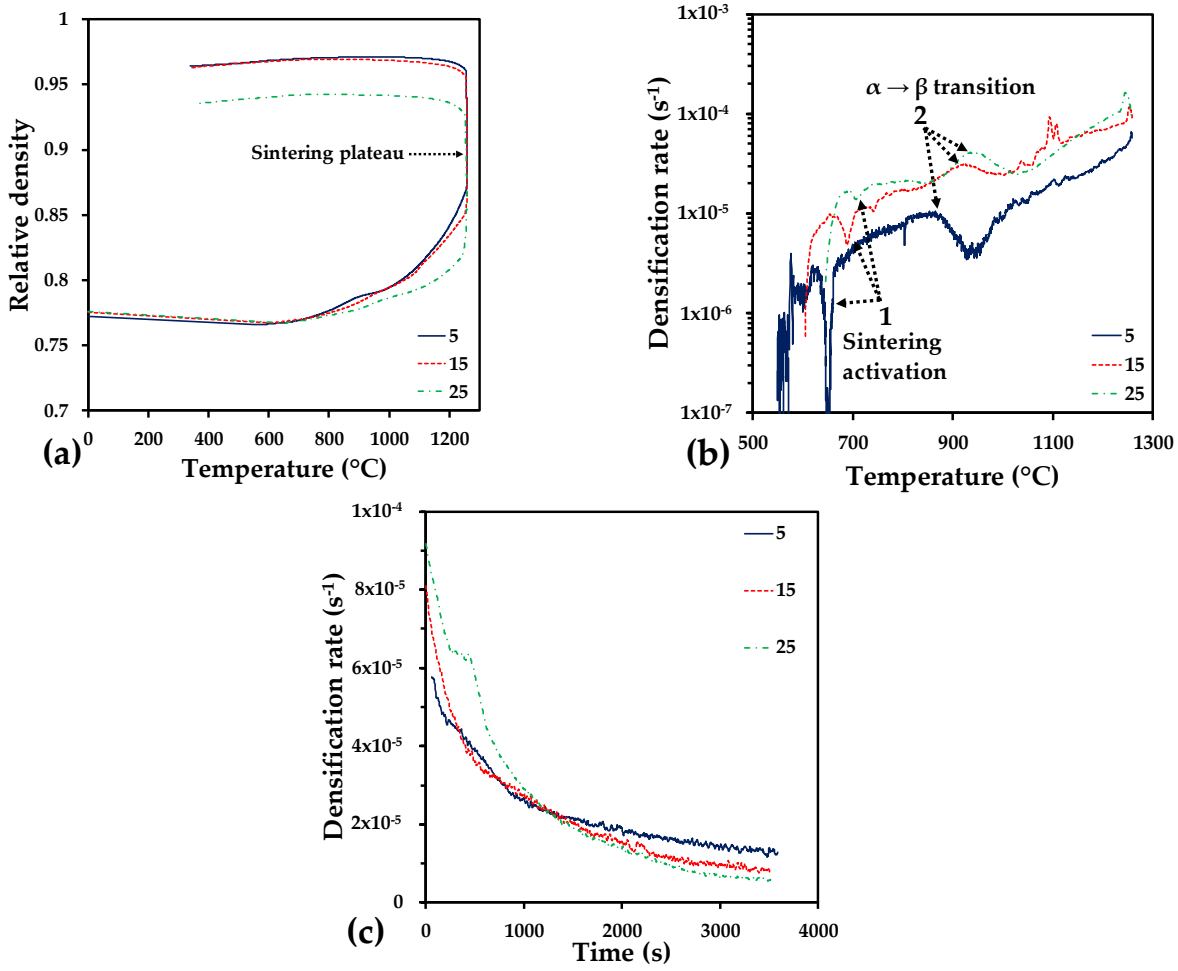

Figure 2. Relative density as a function of temperature during the whole sintering cycle (**a**), densification rate as a function of the temperature during the heating stage (**b**) and densification rate as a function of time during isothermal sintering (**c**).

As expected, the relative density increased during the whole sintering cycle. After a maximum value on densification rate was reached, a reduction on densification rate was found at 860 °C for the sample heated at 5 °C/min (point 2, Figure 2b). This is associated to the $\alpha \rightarrow \beta$ phase transition of the titanium, which is close to that reported in the phase diagram of Ti (882 °C) [26]. As for the sintering activation, the $\alpha \rightarrow \beta$ transition is retarded by an increment in the heating rate, 904 °C and 937 °C for 15 and 25 °C/min, respectively. Then, the densification rate increases until the sintering plateau is reached (1260 °C). As expected, the densification during heating is improved by slow heating and because of that, the relative density reached at the beginning of the plateau is higher for the slow heating rate, 87% for the lowest rate and 83% for the highest one. Then, the relative density increases during the sintering plateau, reaching similar values for heating rates of 5 and 15 °C/min, 97% and 94% for the sample heated at 25 °C/min.

The densification rate during isothermal sintering shows a sharp reduction in the first 1500 s following a logarithmic trend, Figure 2c. After this time, the densification rate is similar for all samples no matter the relative density reached. This behavior suggest that longer times will increase by a small quantity the densification of samples and probably with an excessive increment in the grain size.

The mass diffusion during solid state sintering is mainly achieved by surface and volume diffusion. The first one is considered for the early sintering step, since the neck formation is reached but without densification. Therefore, the volume diffusion is responsible for the densification, and the main diffusion mechanisms driving the densification in Ti have been reported as lattice self-diffusion or grain boundary diffusion [27–29]. Thus, to determine the diffusion mechanism during solid state sintering of the Ti12.5Ta12.5Nb powder mixture, the activation energy should be estimated. According to Liu et al. [30], the following equation can be used when the volume diffusion (VD) or grain boundary diffusion (GBD) are the dominant densification mechanism:

$$ln\left(-T\frac{dl}{l_0 dt}\right) = -\frac{Q}{RT} + ln\left(\frac{AD_0F(\rho)}{G^m}\right) \quad (6)$$

where in l and l_0 are the instantaneous and initial length of the compact, t is the time, D_0 is the diffusion coefficient, G is the grain or particle diameter, m is an index, m = 3 for VD and m = 4 for GBD, $F(\rho)$ is a function of density, R is the universal gas constant, A is a material constant, Q is the activation energy, and T is the absolute temperature. The values of the temperature and deformation rate (dl/l_0dt) at the same density, obtained from the dilatometry data, but sintered at different heating rates, are used to estimate the activation energy. Then, activation energy can be estimated from a linear fit of the Arrhenius plot of the left hand of Equation (5) versus the inverse of the temperature as depicted in Figure 3. The Q values show a sharp increment from around 150 kJ/mol to 260 kJ/mol when the relative density increases to 82%. The Q values determined are at temperatures during the $\alpha \rightarrow \beta$ transition and when the β phase is stabilized. The value of 150 kJ/mol is close to the one reported for grain boundary self-diffusion for β-Ti [27–29,31]. However, the value of 260 kJ/mol is close to the one reported for sintering Ti6Al4V powders, and it was concluded that the main diffusion mechanism is lattice diffusion [22,32]. This increment could be also due to the diffusion of Ta and Nb atoms into the Ti since the diffusion is more active when Ti has the same cubic crystalline structure (β-Ti). An increment in the activation energy has been reported for binary Ti-Ta and Ti-Nb alloys [33]. The values found by Wang et al. for Ti-Ta ranged from 185 to 227 kJ/mol and for Ti-Nb were from 124 to 211 kJ/mol, which are close to the ones obtained in here for the ternary Ti12.5Ta12.5Nb alloy. Based on the above discussed, it can be deduced that densification is driven by lattice diffusion, in where, solid diffusion of Ta and Nb is driven through the necks at the contacts with Ti particles. Therefore, the Ta and Nb particles can be diffused in solid state and remain in the crystalline of titanium.

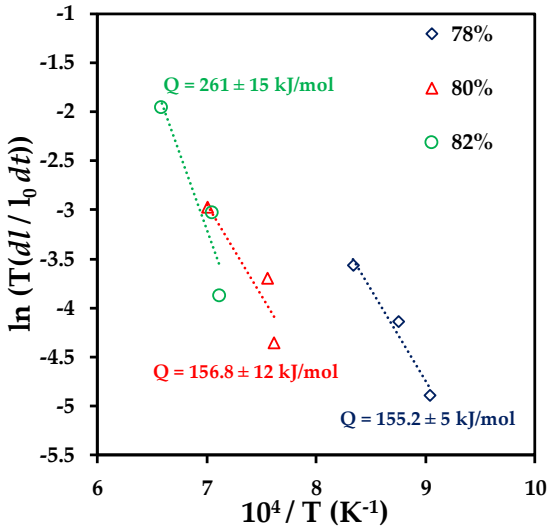

Figure 3. Arrhenius plot of ln (T (dl/l_0dt)) versus the inverse of absolute temperature (T) at different relative densities.

3.2. Microstructure Analysis

3.2.1. XRD Analysis

The microstructure of Ti12.5Ta12.5Nb sintered samples is composed of α, β, α′ and α″ phases, which depends on the heating rate used. As the Ta and Nb are β stabilizer elements, a great amount of these phases are found after sintering. The identification of peaks in the X-ray diffraction patterns (Figure 4) corresponding to the different phases were based in previous works of Ti-Ta, Ti-Nb and Ti-Ta-Nb alloys [34–40]. It was interesting to found that microstructure of samples sintered at 25 °C/min is mostly composed of β-Ti and the martensite phase α″-Ti. Meanwhile, the β-Ti is reduced as the heating rate does it, finding a microstructure composed by α-Ti, β-Ti and the martensite phase of α′-Ti in similar proportions.

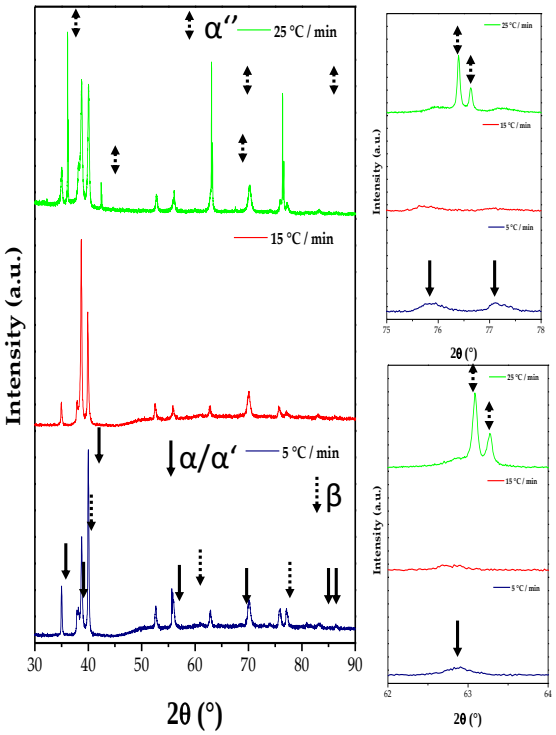

Figure 4. X ray patterns of the samples sintered at 1260 °C with different heating rate.

3.2.2. SEM Microstructure Observation

The microstructure of the Ti12.5Ta12.5Nb shows β-Ti grain with α-Ti segregated at the grain boundaries no matter the heating rate used, Figure 5. Two main features can be distinguished from SEM images generated by the heating rate; the first one is that more pores can be observed as the heating rate increased, Figure 5a–c. However, all pores seem to be isolated and with nearly spherical shape, which confirms the high relative density measured by dilatometry. The second is that grain size seems to be larger as the heating rate slowed, Figure 5a–c. This could be associated with the isothermal sintering, because the sample heated at the lowest rate reached the sintering plateau at a high relative density, thus, most of the isothermal sintering allows grain growth. The grain size was quantitatively measured from a few backscattering SEM images by using the image J software and taking to account the Ferret diameter. As the α-Ti phase is located at the grain boundaries, the difference in contrast generated in the images allows to find the grain limits. It was calculated that the average grain size increased from 47 to 64 μm (Table 1) by reducing the heating rate from 25 to 5 °C/min. The grain size is also influenced by the diffusion of Ta and Nb into the Ti since they stabilize the β. From Figure 5d,e, it is possible to note that close to the Nb and Ta particles the main phase is β, however, a lamellar microstructure starts to be appreciated as the distance from the Ta and Nb particle is made. This was expected, since the diffusion of Ta or Nb is low to homogenize the whole sample during sintering. Another important finding was that martensitic phases nucleated inside the β phase, as shown in Figure 5f. This fact confirms the X-ray diffraction patterns. The martensite phases are obtained during cooling after sintering, because the Ta and Nb atoms inhibit the transition from β → α, so a great amount of martensite phases could be obtained without a quenching treatment. The quantity of β and α phases was also estimated from the SEM images. The quantification was performed by segmenting the gray level in SEM images by using the image J software. In where, light grey is the β phase and the dark gray are the α, α′ and α″ phases. Unfortunately, this method does not separate α, α′, and α″ phases because they show similar grey intensity in the images as the α phase, as discussed, and thus, it is not possible to quantitatively measure the martensitic phases from SEM images. It was found that β-Ti increased with the heating rate, see Table 1. This could be due to the mobility of Ta and Nb atoms inside the Ti cell since most of the time is needed to homogenize the microstructure. Thus, higher heating rate reduced the time of the whole sintering cycle, which generates Ta-rich zones of Ta and Nb atoms. This stabilizes the β phase during cooling or inhibits the complete transition β → α obtaining the metastable martensitic phases.

Table 1. Quantity of Ti-phases after sintering and grain size at different heating rates of Ti12.5Ta12.5Nb.

Heating Rate (°C/min)	α/α′/α″-Ti (%)	β-Ti(%)	Average Grain Size (μm)
5	51.23	46.68	64.78
15	46.29	50.88	50.24
25	39.57	53.42	47.23

3.2.3. EDS Microstructure Analysis

The diffusion of Ta and Nb in the Ti matrix was randomly distributed, which confirms the β-Ti phase stabilization as discussed above. It can also be noticed that α-Ti phase is segregated at the grain boundaries where only Ti is detected by the EDS mapping analysis, Figure 6.

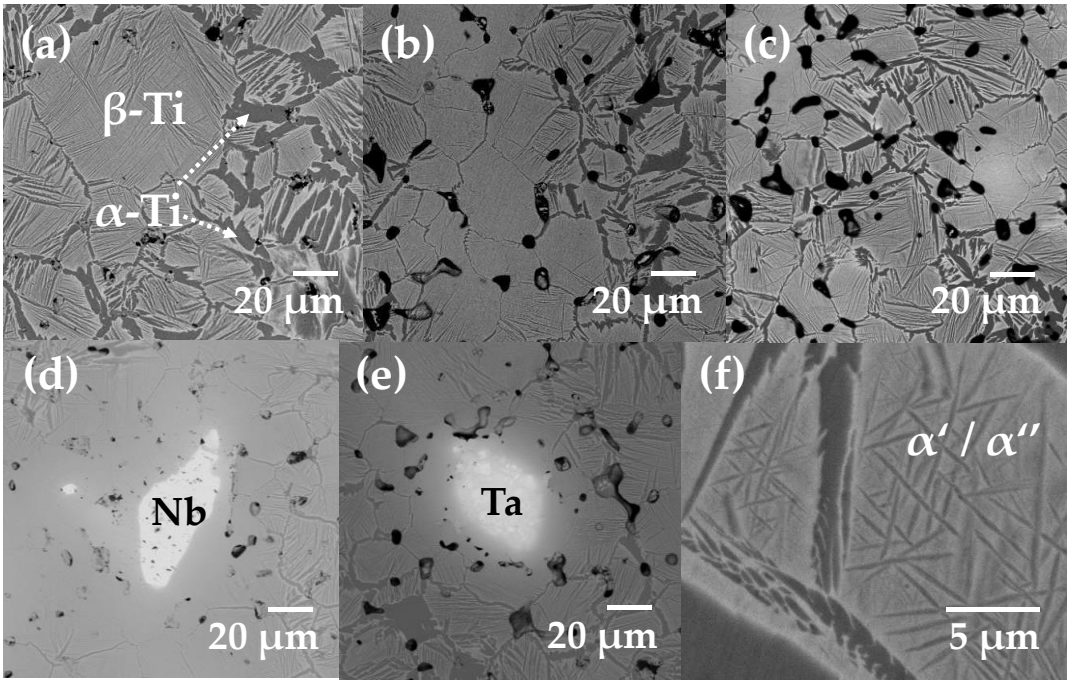

Figure 5. SEM micrographs of the samples sintered at different heating rates (**a**) 5 °C/min, (**b**) 15 °C/min and (**c**) 25 °C/min. Images close to the remaining particles showing the neighborhood, (**d**) Nb and (**e**) Ta particles, respectively. Image a higher magnification showing the microstructure of the β-lamellae (**f**).

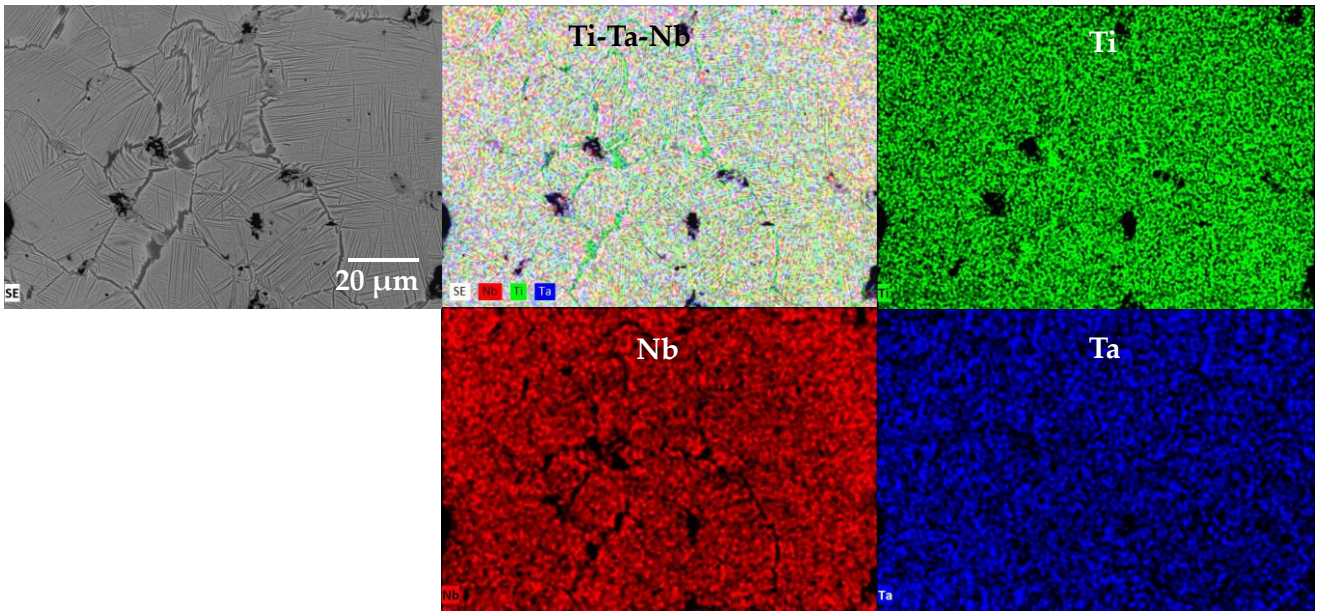

Figure 6. EDS mapping showing the distribution of the elements on the polished surface of the sample sintered at 5 °C/min.

In order to determine the reason of martensitic phase formation an EDS mapping inside of the β-Ti grain was performed. The needle-like microstructure of the martensitic phases can easily be distinguished from Figure 7. As it can be noticed, the Ti is predominant in the thick lamellas (dark gray), which confirms that those are α phase. On the other hand, the composition of the β phase and the martensitic phase show Ti, Ta and Nb distribution that confirms the above discussed. Therefore, the formation of martensitic phases is linked to the Ta or Nb content more than the cooling rate used, as it was reported before [36,41–43].

Thus, the heating rate during sintering plays an important role in the final microstructure, because the longer the thermal cycles, the better Ta and Nb particles diffuse, reducing the formation of martensitic phases.

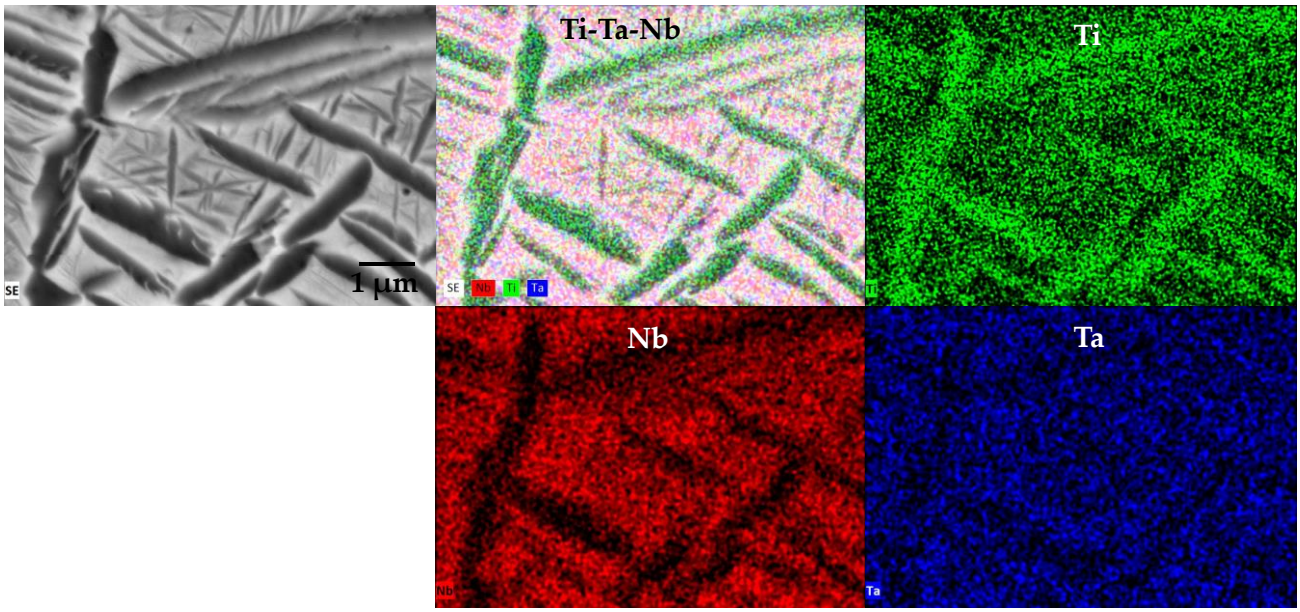

Figure 7. EDS mapping showing the martensitic phase of sample sintered at 25 °C/min.

4. Conclusions

This paper investigated the sintering kinetics and resulting microstructure of a Ti12.5Ta12.5Nb alloy fabricated through powder metallurgy, leading to the following conclusions:

The main diffusion mechanisms are grain boundary and lattice self-diffusion during the $\alpha \rightarrow \beta$ transition and β of Ti. Diffusion at the contacts between Ti-Ta and Ti-Nb was also assumed to occur in the same way since the crystalline structure is cubic for all elements.

Heating rate had a strong effect on the densification and the resulting microstructure, reaching higher relative density and α phase contents as the heating rate slowed.

Metastable α' and α'' were seen because of the saturation of Ta and Nb atoms in the Ti crystalline cell, which inhibits the $\beta \rightarrow \alpha$ transition during the cooling without a higher cooling rate.

The Ti12.5Ta12.5Nb alloy fabricated in this work is promising for use in bone implant applications, since the density of 5.24 g/cm is relatively low. However, analysis of mechanical properties and biocompatibility should be addressed in future studies, in order to fabricate materials with potential use.

Author Contributions: R.M.: Conceptualization; Methodology. P.G.: Project administration; Supervision. C.F.-S.: Experimentation. L.O.: Writing—original draft, Formal analysis. O.J.: Writing—review and editing. M.A.-A.: Validation; Visualization. S.G.-M.: Validation; Supervision. J.L.C.-V.: Formal analysis. All authors have read and agreed to the published version of the manuscript.

Funding: This research received no external funding.

Data Availability Statement: The raw/processed data required to reproduce these findings cannot be shared at this time as the data also forms part of an ongoing study.

Acknowledgments: This research was supported by the National Council for Science and Technology CONACYT via PhD Scholarship of R. Macias (CVU 789772), C. Fernandez-Salvador (791291). The authors would like to thank the CIC of the UMSNH and the National Laboratory SEDEAM-CONACYT, for the financial support and the facilities provided for the development of this study. The authors are grateful for the support provided by the Centro Universitario de Ciencias Exactas e Ingenierías of the Universidad de Guadalajara for the publication of this research.

Conflicts of Interest: The authors declare no conflict of interest.

References

1. Long, M.; Rack, H.J. Titanium alloys in total joint replacement—A materials science perspective. *Biomaterials* **1998**, *19*, 1621–1639. [CrossRef]
2. Wang, X.; Xu, S.; Zhuo, S.; Xu, W.; Leary, M.; Choong, P.; Xie, Y.M. Topological design and additive manufacturing of porous metals for bone scaffolds and orthopaedic implants: A review. *Biomaterials* **2016**, *83*, 127–141. [CrossRef]
3. Niinomi, M. Recent metallic materials for biomedical applications. *Metall. Mater. Trans. A Phys. Metall. Mater. Sci.* **2002**, *33*, 477–486. [CrossRef]
4. Zhou, Z.; Liu, X.; Liu, Q.; Liu, L. Evaluation of the potential cytotoxicity of metals associated with implanted biomaterials (I). *Perp. Biochem. Biotechnol.* **2018**, *39*, 81–91. [CrossRef]
5. Han, M.K.; Kim, J.Y.; Hwang, M.J.; Song, H.J.; Park, Y.J. Effect of Nb on the microstructure, mechanical properties, corrosion behavior, and cytotoxicity of Ti-Nb alloys. *Perp. Biochem. Biotechnol.* **2015**, *8*, 5986–6003. [CrossRef]
6. Zhou, Y.L.; Niinomi, M.; Akahori, T. Changes in mechanical properties of Ti alloys in relation to alloying additions of Ta and Hf. *Mater. Sci. Eng. A* **2008**, *483*, 153–156. [CrossRef]
7. Liu, J.; Chang, L.; Liu, H.; Li, Y.; Yang, H.; Ruan, J. Microstructure, mechanical behavior and biocompatibility of powder metallurgy Nb-Ti-Ta alloys as biomedical material. *Mater. Sci. Eng. C* **2017**, *71*, 512–519. [CrossRef]
8. Zhou, Y.L.; Niinomi, M. Ti–25Ta alloy with the best mechanical compatibility in Ti–Ta alloys for biomedical applications. *Mater. Sci. Eng. C* **2009**, *29*, 1061–1065. [CrossRef]
9. Filip, R.; Kubiak, K.; Ziaja, W.; Sieniawski, J. The effect of microstructure on the mechanical properties of two-phase titanium alloys. *J. Mater. Process. Technol.* **2003**, *133*, 84–89. [CrossRef]
10. Macias, R.; Garnica-Gonzalez, P.; Olmos, L.; Jimenez, O.; Chavez, J.; Vazquez, O.; Arteaga, D. Sintering Analysis of Porous Ti/xTa Alloys Fabricated from Elemental Powders. *Materials* **2022**, *15*, 6548. [CrossRef]
11. Correa, D.R.N.; Kuroda, P.A.B.; Lourenco, M.L.; Fernandes, C.J.C.; Buzalaf, M.A.R.; Zambuzzi, W.F.; Grandini, C.R. Development of Ti-15Zr-Mo alloys for applying as implantable biomedical devices. *J. Alloys Compd.* **2018**, *749*, 163–171. [CrossRef]
12. Kuroda, P.A.B.; Quadros, F.D.F.; Araújo, R.O.D.; Afonso, C.R.M.; Grandini, C.R. Effect of thermomechanical treatments on the phases, microstructure, microhardness and young's modulus of ti-25ta-zr alloys. *Materials* **2019**, *12*, 3210. [CrossRef]
13. Li, P.; Ma, X.; Wang, D.; Zhang, H. Microstructural and mechanical properties of β-type Ti–Nb–Sn biomedical alloys with low elastic modulus. *Metals* **2019**, *9*, 712. [CrossRef]
14. Olmos, L.; Cabezas-Villa, J.L.; Bouvard, D.; Lemus-Ruiz, J.; Jiménez, O.; Falcón-Franco, L.A. Synthesis and characterisation of Ti6Al4V/xTa alloy processed by solid state sintering. *Powder Metall.* **2020**, *63*, 64–74. [CrossRef]
15. Mediaswanti, K.; Wen, C.; Ivanova, E.P.; Berndt, C.C.; Wang, J. Sputtered hydroxyapatite nanocoatings on novel titanium alloys for biomedical applications. In *Titanium Alloys—Advances in Properties Control*, 1st ed.; Sieniawski, J., Ziaja, W., Eds.; Intech open: Vienna, Austria, 2013; pp. 21–44. [CrossRef]
16. Zhou, Y.L.; Niinomi, M. Microstructures and mechanical properties of Ti–50 mass% Ta alloy for biomedical applications. *J. Alloys Compd.* **2008**, *466*, 535–542. [CrossRef]
17. Zhou, Y.L.; Niinomi, M.; Akahori, T. Effects of Ta content on Young's modulus and tensile properties of binary Ti–Ta alloys for biomedical applications. *Mater. Sci. Eng. A* **2004**, *371*, 283–290. [CrossRef]
18. Gordin, D.M.; Delvat, E.; Chelariu, R.; Ungureanu, G.; Besse, M.; Laile, D.; Gloriant, T. Characterization of Ti-Ta Alloys Synthesized by Cold Crucible Levitation Melting. *Adv. Eng. Mater.* **2008**, *10*, 714–719. [CrossRef]
19. Niinomi, M. Mechanical properties of biomedical titanium alloys. *Mater. Sci. Eng. A* **1998**, *243*, 231–236. [CrossRef]
20. Gepreel, M.A.H.; Niinomi, M. Biocompatibility of Ti-alloys for long-term implantation. *J. Mech Behav. Biomed. Mater.* **2013**, *20*, 407–415. [CrossRef]
21. Hussein, A.H.; Gepreel, M.A.H.; Gouda, M.K.; Hefnawy, A.M.; Kandil, S.H. Biocompatibility of new Ti–Nb–Ta base alloys. *Mater. Sci. Eng. C* **2016**, *61*, 574–578. [CrossRef]
22. Cabezas-Villa, J.; Lemus-Ruiz, J.; Bouvard, D.; Jiménez, O.; Vergara-Hernández, H.J.; Olmos, L. Sintering study of Ti6Al4V powders with different particle sizes and their mechanical properties. *Int. J. Miner. Metall. Mater.* **2018**, *25*, 1389–1401. [CrossRef]
23. Garnica, P.; Macías, R.; Chávez, J.; Bouvard, D.; Jiménez, O.; Arteaga, D. Fabrication and characterization of highly porous Ti6Al4V/xTa composites for orthopedic applications. *J. Mater. Sci.* **2020**, *55*, 16419–16431. [CrossRef]
24. Karre, R.; Niranjan, M.K.; Dey, S.R. First principles theoretical investigations of low Young's modulus beta Ti–Nb and Ti–Nb–Zr alloys compositions for biomedical applications. *Mater. Sci. Eng. C* **2015**, *50*, 52–58. [CrossRef]

25. Zhuravleva, K.; Bönisch, M.; Scudino, S.; Calin, M.; Schultz, L.; Eckert, J.; Gebert, A. Phase transformations in ball-milled Ti–40Nb and Ti–45Nb powders upon quenching from the ß-phase region. *Powder Technol.* **2014**, *253*, 166–171. [CrossRef]
26. Murray, J.L. The Ta− Ti (Tantalum-Titanium) system. *Bull. Alloy. Phase Diagr.* **1981**, *2*, 62–66. [CrossRef]
27. German, R.M. Titanium sintering science: A review of atomic events during densification. *Int. J. Refract. Hard. Met.* **2020**, *89*, 105214. [CrossRef]
28. Chen, T.; Yang, C.; Liu, Z.; Ma, H.W.; Kang, L.M.; Wang, Z.; Li, Y.Y. Revealing dehydrogenation effect and resultant densification mechanism during pressureless sintering of TiH2 powder. *J. Alloys Compd.* **2021**, *873*, 159792. [CrossRef]
29. Panigrahi, B.B.; Godkhindi, M.M.; Das, K.; Mukunda, P.G.; Ramakrishnan, P. Sintering kinetics of micrometric titanium powder. *Mater. Sci. Eng. A* **2005**, *396*, 255–262. [CrossRef]
30. Liu, Z.Y.; Loh, N.H.; Khor, K.A.; Tor, S.B. Sintering activation energy of powder injection molded 316L stainless steel. *Scr. Mater.* **2001**, *44*, 1131–1137. [CrossRef]
31. Herzig, C.; Wilger, T.; Przeorski, T.; Hisker, F.; Divinski, S. Titanium tracer diffusion in grain boundaries of α-Ti, α2-Ti3Al, and γ-TiAl and in α2/γ interphase boundaries. *Intermetallics* **2001**, *9*, 431–442. [CrossRef]
32. Xu, X.; Nash, P. Sintering mechanisms of Armstrong prealloyed Ti–6Al–4V powders. *Mater. Sci. Eng. A* **2014**, *607*, 409–416. [CrossRef]
33. Wang, K.; Liu, X.; Liu, T.; He, C.; Liu, J. Investigation on Diffusion Kinetics of Ti-X Binary Systems at 1300–1500 °C. *Available SSRN 4440837*. [CrossRef]
34. Huang, S.; Sing, S.L.; de Looze, G.; Wilson, R.; Yeong, W.Y. Laser powder bed fusion of titanium-tantalum alloys: Compositions and designs for biomedical applications. *J. Mech. Behav. Mater.* **2020**, *108*, 103775. [CrossRef]
35. Ma, Y.Q.; Jin, W.J.; Yang, S.Y.; Zhang, J.B.; Huang, Y.X.; Liu, X.J. Microstructure and shape memory properties of biomedical Ti-(40-65) Ta (wt.%) alloys. In *Materials Science Forum*; Trans Tech Publications Ltd.: Stafa-Zurich, Switzerland, 2009; Volume 610, pp. 1382–1386. [CrossRef]
36. Yi, X.; Sun, K.; Liu, J.; Zheng, X.; Meng, X.; Gao, Z.; Cai, W. Tailoring the microstructure, martensitic transformation and strain recovery characteristics of Ti-Ta shape memory alloys by changing Hf content. *J. Mater. Sci. Technol.* **2021**, *83*, 123–130. [CrossRef]
37. Fikeni, L.; Annan, K.A.; Mutombo, K.; Machaka, R. Effect of Nb content on the microstructure and mechanical properties of binary Ti-Nb alloys. *Mater. Today Proc.* **2021**, *38*, 913–917. [CrossRef]
38. Dutkiewicz, J.; Kuśnierz, J.; Maziarz, W.; Lejkowska, M.; Garbacz, H.; Lewandowska, M.; Kurzydłowski, K.J. Microstructure and mechanical properties of nanocrystalline titanium and Ti–Ta–Nb alloy manufactured using various deformation methods. *Phys. Satus. Solidi.* **2005**, *202*, 2309–2320. [CrossRef]
39. Silva, K.B.D.; Carobolante, J.P.A.; Rajan, S.S.; Júnior, C.B.; Sabino, R.M.; Seixas, M.R.; Claro, A.P.R.A. Mechanical Properties, Corrosion Behavior, and In Vitro Cell Studies of the New Ti-25Ta-25Nb-5Sn Alloy. *Materials* **2023**, *16*, 1970. [CrossRef]
40. Voňavková, I.; Průša, F.; Kubásek, J.; Michalcová, A.; Vojtěch, D. Microstructure and Mechanical Properties of Ti-25Nb-4Ta-8Sn Alloy Prepared by Spark Plasma Sintering. *Materials* **2022**, *15*, 2158. [CrossRef]
41. Dobromyslov, A.V.; Elkin, V.A. Martensitic transformation and metastable β-phase in binary titanium alloys with d-metals of 4–6 periods. *Scripta Mater.* **2001**, *44*, 905–910. [CrossRef]
42. Paulsen, A.; Frenzel, J.; Langenkämper, D.; Rynko, R.; Kadletz, P.; Grossmann, L.; Eggeler, G. A kinetic study on the evolution of martensitic transformation behavior and microstructures in Ti–Ta high-temperature shape-memory alloys during aging. *Shap. Mem. Superelasticity* **2019**, *5*, 16–31. [CrossRef]
43. Kalita, D.; Rogal, Ł.; Berent, K.; Góral, A.; Dutkiewicz, J. Effect of Mo and Ta on the mechanical and superelastic properties of Ti-Nb alloys prepared by mechanical alloying and spark plasma sintering. *Materials* **2021**, *14*, 2619. [CrossRef] [PubMed]

Disclaimer/Publisher's Note: The statements, opinions and data contained in all publications are solely those of the individual author(s) and contributor(s) and not of MDPI and/or the editor(s). MDPI and/or the editor(s) disclaim responsibility for any injury to people or property resulting from any ideas, methods, instructions or products referred to in the content.